A Numerical Study of Axi-symmetric Droplet Formation Using A Moving Mesh Approach

Sandeep Menon, Jonathan Rothstein and David P. Schmidt*
Department of Mechanical and Industrial Engineering
University of Massachusetts Amherst
Amherst, MA 01003

Abstract

Interface tracking techniques, used in conjunction with finite volume methods to study droplet formation, have gained recent popularity, particularly at low and moderate Weber numbers. Simulations of interface behavior using moving and deforming meshes are particularly difficult, since the quality of the underlying mesh must be maintained to obtain high solution accuracy. This paper addresses a few of the common challenges associated with such methods, using simulations involving liquid break-up in axi-symmetric cases. Situations involving the manipulation of mesh connectivity and vertex positions are discussed in detail, including an efficient algorithm for the calculation of length scales at any location in the mesh. Additionally, thermally induced variations of fluid properties like viscosity, surface-tension (Marangoni surface stress) and non-Newtonian effects are incorporated to study droplet formation and behavior. Results of these simulations are useful in the study of Drop-on-Demand ink-Jet printing applications.

Introduction

Ink-jet printing has matured to a level where it finds widespread use in several areas of modern technology, including printed electronics, microarray fabrication and large-scale paper-based printing. In the past, the development of systems employed for ink-jet printing relied largely on prototyping, which quickly proved to be expensive. The numerical study of droplet formation is therefore particularly attractive to researchers who develop such technologies, since it contributes significantly towards shorter development cycles, in addition to the obvious cost benefits. Simulations of multiphase fluid flow is divided broadly into two categories: interface capturing and interface tracking methods.

Interface capturing methods describe a general class of techniques which approximate the fluid interface to a finite thickness. Examples of these techniques are the Volume-of-fluids (VOF), Level Set and Lattice Boltzmann (LBM) methods. The VOF approach uses a color function at each cell on a fixed mesh to define the volume fraction of the two fluids. This function is then advected with a conservative flux-limiting scheme to describe the transient behavior of the interface. Naive implementations of VOF suffer from interface smearing effects, which can be overcome by the Piecewise Linear Interface Construction (PLIC) approach, resulting in a sharp, albeit discontinuous, interface. Surface tension forces are then typically evaluated by the Continuum Surface Force (CSF) method by Brackbill et al [1, 2]. Level Set methods possess challenges in mass-conservation, but have also been shown to be a particularly fast technique. When used in conjunction with immersed interface methods, the Level Set approach can be used to track sharp interfaces [3]. Parallelization of VOF and level-set methods for large calculations has also been very successful [4]. Lattice Boltzmann methods have also been applied to multiphase flows, where forces due to particle interactions are particularly useful when modeling surface-tension [5]. However, these methods have limitations when jump conditions are applied at interfaces, and applicability to generalized flows is difficult.

Lagrangian methods (first introduced by Harlow and Welch [6]) directly track the interface motion using the local fluid velocity. The mesh adapts as the interface evolves so that cell faces remain coincident with the fluid interface. Examples are past work by Helenbrook [7], Wadhwa [8], Cristini [9], and Quan [10]. This approach is particularly attractive since the interface is not smeared and so, interface reconstruction is unnecessary. It also allows jump conditions across the interface to be applied directly. Mesh-resolution at the interface can also be carefully controlled by continuous adaptation, and consequently, surface curvature (and therefore, surface tension) can be calculated accurately.

Interface tracking has to be done carefully, since excessive mesh deformation quickly leads to highly skewed cells, which are detrimental to numerical accuracy. Global remeshing is prohibitively expensive in such cases. On the other hand, local remeshing of areas containing poor quality cells shows an immediate benefit of computational cost, in addition to limiting interpolation errors to the region. Cases involving droplet breakup and coalescence is particularly

*Corresponding author

challenging in interface tracking methods, since cells in the pinching region must be manipulated to account for a change in interface topology.

Governing equations

The moving, deforming mesh requires a more general control volume treatment. The governing equations of an incompressible fluid for an arbitrary moving control volume V, bounded by a surface S and normal $\mathbf{n}$ are:

$$\oint_S \mathbf{u}\cdot\mathbf{n}\,dS = 0 \tag{1a}$$

$$\frac{d}{dt}\int_V \rho\mathbf{u}\,dV + \oint_S \rho\mathbf{u}\,(\mathbf{u}-\mathbf{u}_b)\cdot\mathbf{n}\,dS = -\int_V \nabla p\,dV + \oint_S \mu\nabla\mathbf{u}\,dS \tag{1b}$$

where $\mathbf{u}$ and $\mathbf{u}_b$ are the fluid and mesh velocities, respectively; μ is the molecular viscosity, and ρ is the density of the fluid. The equations for the moving control volume are additionally constrained by the space-conservation law, which is obtained using the Leibniz theorem:

$$\frac{d}{dt}\int dV = \oint_S \mathbf{u}_b\cdot\mathbf{n}\,dS \tag{2}$$

It is also convenient to define the face-normal components of the fluid and mesh velocity:

$$U_f = \oint_S \mathbf{u}\cdot\mathbf{n}\,dS \tag{3a}$$

$$U_{mesh} = \oint_S \mathbf{u}_b\cdot\mathbf{n}\,dS \tag{3b}$$

In the discrete sense, Eq.(2) relates the change in volume of the element to the volume swept by its faces during the time-step, which must be enforced to machine accuracy [11]:

$$\frac{V^{n+1}-V^n}{\Delta t} = \sum_{faces} U_{mesh} \tag{4}$$

The momentum equations are discretized using a collocated arrangement for the pressure and velocity variables at element centres, and the pressure-velocity coupling is handled in a segregated manner using the PISO algorithm by Issa [12]. In this approach, the convection term is linearized so that the existing velocity fluxes are used to calculate the new velocity at the next time-step:

$$\nabla\cdot(\mathbf{UU}) = \sum_{faces}\left(U_f^n\cdot\mathbf{n}\right)U_f^{n+1} \tag{5a}$$

$$= \sum_{faces}\phi\,U_f^{n+1} \tag{5b}$$

where ϕ is the divergence-free velocity flux at the existing time-step. Following this, the existing pressure gradient field is used to predict the velocity field at the new time. The Poisson equation for pressure is then solved using this new velocity field, followed in sequence by corrections to the velocity, until the fluxes are divergence-free. Surface-tension effects appear as boundary conditions on the free-surface. This is given by:

$$-p\mathbf{n} + \mu\left(\nabla\mathbf{u}+\nabla\mathbf{u}^T\right)\cdot\mathbf{n} = \frac{\sigma}{R}\mathbf{n} \tag{6}$$

where σ is the surface tension and R is the radius of curvature at the interface. For an interface involving two fluids, this relation is given as:

$$\langle -p\mathbf{n} + \mu\left(\nabla\mathbf{u}+\nabla\mathbf{u}^T\right)\cdot\mathbf{n}\rangle = \frac{\sigma}{R}\mathbf{n} \tag{7}$$

where $\langle\cdot\rangle$ represents a difference across the interface: $(.)_{liquid} - (.)_{gas}$.

Non-newtonian fluids exhibit viscosities that depend on the strain-rate of the fluid and so, corrections must be made to the viscosity as the simulation progresses. This kind of behavior is reproduced fairly well by the Bird-Carreau model [13], which is given by the following constitutive relation:

$$\left(\frac{\eta-\eta_\infty}{\eta_o-\eta_\infty}\right) = \left[\frac{1}{1+(\lambda\dot{\gamma})^2}\right]^{\left(\frac{1-n}{2}\right)} \tag{8}$$

The model contains four parameters: the zero strain-rate viscosity η_o, infinite strain-rate viscosity η_∞, viscoelastic time constant λ, and a dimensionless constant n - which describes the slope of the power-law region of log η vs. log $\dot{\gamma}$, where $\dot{\gamma}$ is the strain-rate and is given by $|\nabla \mathbf{u}|$. Here, η is defined as (μ/ρ) for convenience.

Variations in viscosity due to fluid temperature are modeled using the Vogel-Fulcher-Tammann (VFT) relation [14]:

$$\eta = \eta_o \, exp\left[a\left(\frac{T_o}{T-b} - c\right)\right] \tag{9a}$$

$$a = \left(\frac{T_A}{T_o}\right) \tag{9b}$$

$$b = T_V \tag{9c}$$

$$c = \frac{T_o}{T_o - T_V} \tag{9d}$$

where η_o, T_o, T_V and T_A are the reference viscosity, reference temperature, Vogel and activation temperatures, respectively. In this work, these values were set to be: $\eta_o = 10^{-6}$, $T_o = 298.15K$, $T_V = 156.8K$ and $T_A = 937.38K$.

In accordance with the Eötvos rule, surface tension varies linearly with temperature, and is described by the following relation:

$$\sigma = \sigma_o - \beta\,(T - T_o) \tag{10}$$

In this work, these values were: $\sigma_o = 72.7\ dyne/cm$, $\beta = 0.18\ dyne/cm/K$ and $T_o = 298K$.

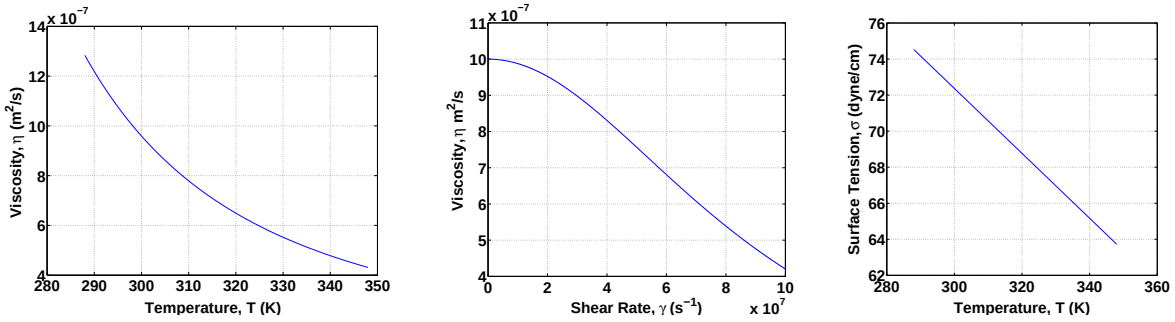

(a) Viscosity with Temperature (b) Viscosity with Shear rate (c) Surface tension with Temperature

Figure 1: Variation of fluid properties

Mesh motion and reconnection

While Lagrangian tracking updates interface vertices explicitly, interior vertices are positioned in a manner that maximizes the quality of cells in the mesh. This movement of mesh vertices is reflected in the application of the Reynolds transport theorem to the conservation laws. In this work, the spring-analogy method (weighted Laplacian mesh motion) is used to update vertex positions, described by the equation:

$$\sum_j k_{ij}(\mathbf{x}_{ij} - \mathbf{x}_i) = 0 \tag{11}$$

where $\mathbf{x}_i$ denotes the position of an interior free-vertex in the mesh, and $\mathbf{x}_{ij}$ denotes the positions of its immediate neighbors. The weighting, k_{ij}, represents a spring-stiffness. When k_{ij} is equal to the inverse length of the edge, it makes shorter edges stiff, but also introduces a small amount of non-linearity into the problem. In this work, k_{ij} was set to unity. This approach yields a symmetric positive-definite system of equations, which can be solved quickly using an iterative solver like the Conjugate Gradient method.

In two-dimensional simplical meshes, three basic operations for connectivity modifications are defined, as shown in Fig. 2. The Delaunay criterion (for 2D) plainly states that any vertex must not be contained within the circumcircle of any triangle in the mesh. In situations of large mesh deformation, neighboring vertices may move prohibitively far

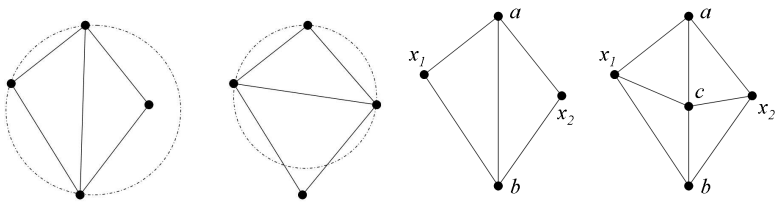

(a) Delaunay Flipping (b) Edge Bisection: Edge *ab* is bisected at vertex *c*

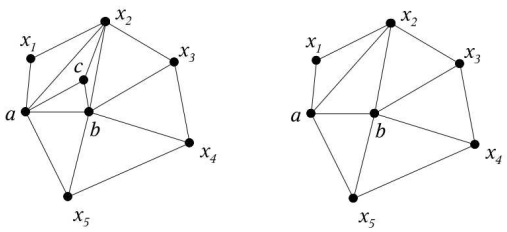

(c) Edge Collapse: Edge *bc* is collapsed to vertex *b*

Figure 2: Mesh topology modifications

apart or may become nearly co-located. In these cases, the edge bisection and collapse operations must be applied to maintain quality. These topological operations can also be used to maintain maximal and minimal length-scales at any location in the mesh. This is particularly useful since the mesh size dictates the maximum Courant number observed during the simulation, which is closely related to numerical stability. Length scales in the mesh are defined by a greedy algorithm which initializes boundary length-scales first; followed by a multiplicative growth factor for every cell-layer towards the interior of the mesh. This allows the mesh to be reasonably coarse toward the mesh interior, thereby allowing substantial savings in computational cost. In axi-symmetric simulations involving only one phase, pinch-off is implemented by collapsing edges preferentially towards the centerline.

Modeling results and discussion

This section shows the results obtained from simulations subjected to several parametric variations. These cases involve only the liquid phase, and effects of the gas-phase, though significant, are currently neglected. Unless stated otherwise, the fixed system conditions are as follows: Inlet jet velocity of 20 m/s; an orifice diameter of 8.8 μm. This corresponds to a Weber number (We) of 50.28, and a Capillary number (Ca) of 0.285.

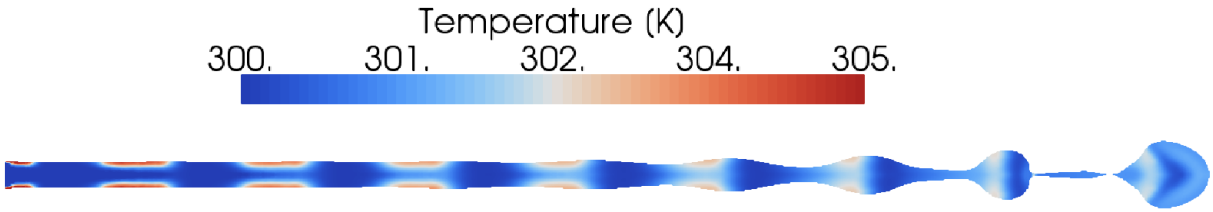

Figure 3: Thermal modulation of a continuous inkjet, shown at 5.5μs after start of injection

Pressure modulation

Drop-on-demand methods for inkjet printing always employ some form of pressure modulation to achieve droplets, including bubble-jets, piezoelectric, or diaphragm-based actuation. The quantity of ink dispensed from the orifice is dependent on the duration of the pressure pulse. Depending on the waveform of the actuating signal and various fluid properties, satellite droplet formation can also occur. Satellite droplets are known to be a major cause of inferior print

quality, and careful modulation of properties if often required to avoid them. This is depicted quite clearly in Fig. 4(a), where the tail end of the drop eventually pinches off into a smaller droplet. The inlet is subjected to a fixed velocity of 20 m/s, which is subsequently switched off after 1.4 μs. At this point, surface tension causes necking to occur, and the drop eventually breaks off. Higher values of surface-tension accelerate the time to pinch-off. Higher shear-rates occur in the region around the orifice, causing minor shear-thinning effects with the Bird-Carreau model. This effect modifies the initial flow profile slightly, but does not show any significant changes in drop formation behavior. Non-Newtonian models which capture extensional behavior may influence satellite droplet formation, but their implementation is much more complicated.

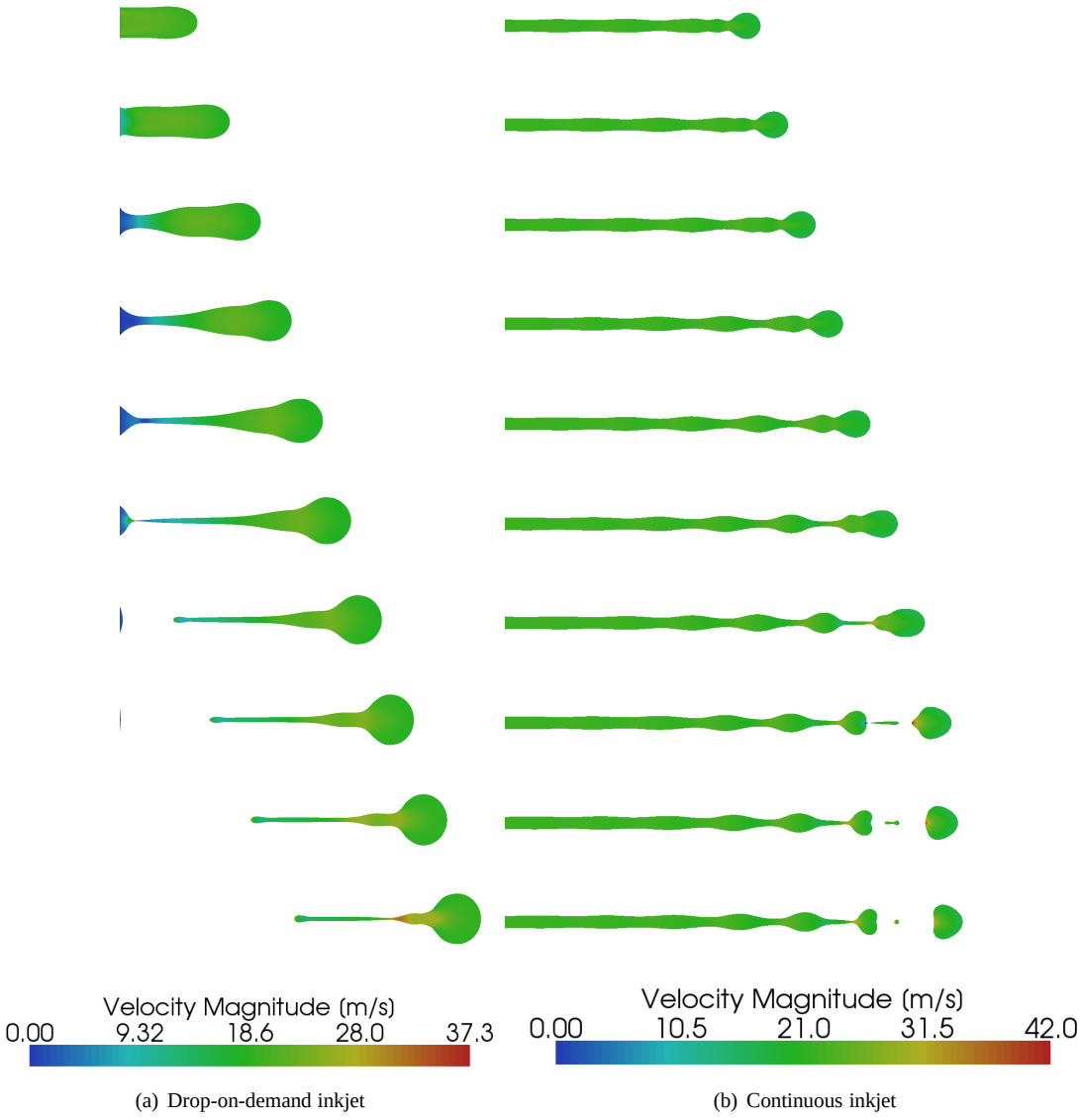

(a) Drop-on-demand inkjet (b) Continuous inkjet

Figure 4: Stages of jet evolution at approx. 0.2μs intervals, starting at 0.7μs after start of injection

Temperature modulation

High speed printing applications frequently require a continuous inkjet approach. In such cases, the formation of instabilities along the length of the jet cause it to break up into drops (and smaller satellite droplets). Most continuous inkjet methods employ thermal modulation to create spatial gradients of surface-tension. The resultant shear-stress

at the interface results in Marangoni flow along the jet, eventually leading to instabilities and droplet formation. Temperature was modulated using a square wave profile. The percentage fraction of the heating pulse period relative to the modulation period is referred to as the duty cycle. In this work, with a period of $2\mu s$, heat was applied at a 50% duty cycle (i.e., for $1\mu s$). Fig. 4(b) shows the evolution of a continuous ink-jet subjected to thermal modulation in the range [300K-350K], set at a frequency of 500 kHz. Temperature contours depicting the thermal modulation is shown in Fig. 3. Choosing larger values for β (in Eq. 10) leads to larger spatial gradients of surface-tension along the jet, leading to a shorter break-off length (BOL). Shorter BOL can also be achieved by increasing the frequency of modulation.

Conclusions

An interface tracking method for two-dimensional axisymmetric flows using the moving mesh technique has been developed, and has been shown to be versatile in handling various regimes of droplet formation in inkjets. In addition to rigorous validation, extension to simulations involving the gas-phase and three-dimensional cases are currently being developed to handle more complicated situations and physics.

Acknowledgements

We acknowledge the technical advice of Dr. Edward Furlani and the financial support of Kodak Inc. We also acknowledge the financial support of the Army Research Office under the supervision of Dr. Ralph Anthenian. We thank Dr. Hrvoje Jasak and Dr. Željko Tuković for their helpful suggestions.

References

[1] J. U. Brackbill, D. B. Kothe, and C. Zemach. *J. Comput. Phys.*, 100(2):335–354, 1992.

[2] S. Afkhami and M. Bussmann. *International Journal for Numerical Methods in Fluids*, 57(4):453–472, 2008.

[3] Z. Li and M.-C. Lai. *Journal of Computational Physics*, 171:822–842, 2001.

[4] E. Aulisa, S. Manservisi, and R. Scardovelli. *Computer Methods in Applied Mechanics and Engineering*, 195(44-47):6239–6257, Sep 2006.

[5] X. He, S. Chen, and R. Zhang. *Journal of Computational Physics*, 152:642–663, 1999.

[6] F. H. Harlow and J. E. Welch. *Physics of fluids*, 8:2182, 1965.

[7] B. T. Helenbrook. In *Proceedings of ILASS Americas 14th Annual Conference on Liquid Atomization and Spray Systems*, pages 123–128. Institute for Liquid Atomization and Spray Systems, May 2001.

[8] A. R. Wadhwa, J. Abraham, and V. Magi. *Journal of the American Institute of Aeronautics and Astronautics*, 43(9):1974–1983, Sep 2005.

[9] V. Cristini, J. Blawzdziewicz, and M. Loeweberg. *Journal of Computational Physics*, 168:445–463, 2001.

[10] S. Quan and D.P. Schmidt. *Journal of Computational Physics*, 221(2):761–780, 2007.

[11] M. Dai and D. P. Schmidt. *Journal of Computational Physics*, 208(1):228–252, 2005.

[12] R. I. Issa. *J. Comput. Phys.*, 62(1):40–65, 1986.

[13] R. B. Bird. *Annual Review of Fluid Mechanics*, 8(1):13–34, 1976.

[14] L. S. Garca-Coln, L. F. del Castillo, and P. Goldstein. *Phys. Rev. B*, 40(10):7040–7044, Oct 1989.